INTERNAL WAVES IN A PYCNOCLINE FOR A WING MOVING OVER A BARRIER

V. I. Bukreev, N. V. Gavrilov, and A. V. Gusev

UDC 532.59

Experiments have been performed on the fundamental physics of wave interaction with an obstacle subject to the following basic features. The medium in which the wave propagates (liquid with continuous density stratification, which is incompressible and at rest in the unperturbed state) is dispersive; the dispersion formula describes the relation between the wave number k and the circular frequency ω in a linear approximation when planar harmonic waves propagate in the medium and has an unbounded but denumerable set of branches $\omega_m(k)$ (m = 0, 1, 2, ...).

That medium provides the basis for an interesting but largely neglected effect: energy redistribution between all eigenmodes when only one of them is excited directly, which is predicted in the linear approximation, i.e., when the perturbation has infinitesimally small energy. That effect occurs in particular when internal waves interact in a continuously stratified liquid with an obstacle placed in it. The theoretical basis for this has been given [1, 2] for the interaction of waves with a barrier in a liquid having an exponential depth density distribution. A survey of other papers can be found in [3]. Here we give a way of providing a theoretical basis for the effect that is not related to any particular density distribution but instead illustrates how it occurs in experiments with internal waves arising from a wing moving over a barrier having a sharp edge or broad threshold.

The continuous displacement of the wing with respect to the obstacle in the experiments led to a nonstationary situation and provides a further distinctive feature. The nonstationary feature is accentuated because the wing is accelerated over a short period from a state of rest and after prolonged uniform motion is halted rapidly. Finally, the nonlinearity in a stratified liquid means that perturbations may propagate far ahead of the wing and be other than single harmonics [4].

1. The experiments were performed in the basin shown schematically in Fig. 1, which had L = 5 m and width B = 0.2 m. The basin was initially partially filled with a solution of glycerol in water having density ρ_1, after which distilled water with density $\rho_2 < \rho_1$ was run onto the surface through Porolon floats. The mixing during the pouring and the molecular diffusion resulted in a density distribution $\rho(y)$:

$$\rho(y) = \rho_0\left(1 - \frac{\varepsilon}{2+\varepsilon}\operatorname{th}\frac{2y}{\delta}\right), \quad \varepsilon = \frac{\rho_1}{\rho_2} - 1, \quad \rho_0 = \frac{\rho_1+\rho_2}{2}. \tag{1.1}$$

Here δ is the width of the diffuse zone and y the vertical coordinate, which is reckoned upwards from the plane on which $\rho = \rho_0$ in the unperturbed state. That plane is called the interface.

We tested (1.1) by experiment with a laser on the basis that any two points 1 and 2 on the beam propagating in a transparent medium with refractive index n(y) will obey $n_1 \sin\theta_1 = n_2 \sin\theta_2$ (θ is the angle between the tangent to the ray and the y axis). This gives a recurrent algorithm that enables one to use the known n_1 and θ_1 with the measured θ_2 to calculate n_2. We converted n(y) to $\rho(y)$ on the basis that $\rho(n)$ is close to linear for small variations in ρ.

The rise in δ with time was quite slow. Measurements showed that δ = 0.9 cm at 0.5 h after the filling, 1.5 cm at 3 h, and 2.8 cm at 19 h. If necessary, δ can be reduced by sucking off the liquid from the diffuse region slowly. The minimum attainable δ was 0.45 cm.

Novosibirsk. Translated from Zhurnal Prikladnoi Mekhaniki i Tekhnicheskoi Fiziki, No. 4, pp. 68-74, July-August, 1991. Original article submitted December 25, 1989; revision submitted April 2, 1990.

 0021-8944/91/3204-0528$12.50

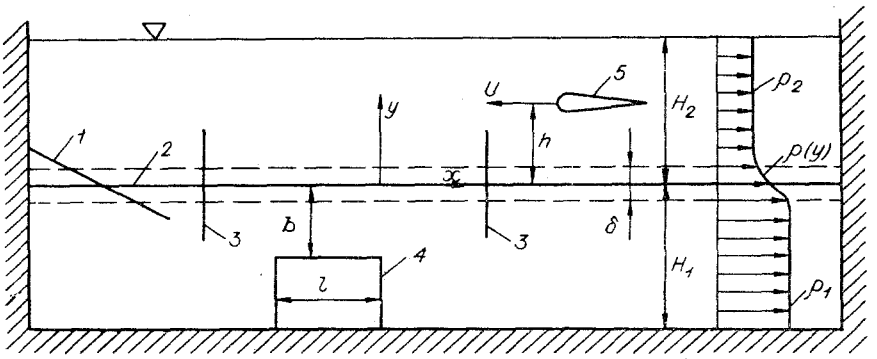

Fig. 1

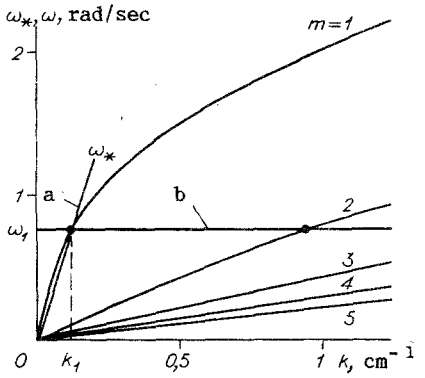

Fig. 2

The barrier 4 (Fig. 1) was placed at the bottom, with the top face at a depth b below the boundary 2. Three experiment series were performed. In one, the barrier had length along the x axis ℓ = 48. 1 cm, and in the second, it was 24.2 cm, while in the third it had a sharp edge ($\ell \to 0$). In the first two cases, the barrier is called a broad threshold, as ℓ is comparable with the wavelength λ of the incident wave. The perturbations were produced by the wing 5, which moved horizontally at zero angle of attack at a distance h = const from the boundary with speed

$$-U = \begin{cases} U_0[1-\exp(-t/\tau_1)] & \text{for } 0 \leqslant t < T, \\ U_0 \exp(-t/\tau_2) & \text{for } t \geqslant T \end{cases} \qquad (1.2)$$

(t is time, while U_0, T, τ_1, and τ_2 are parameters). Here τ_1 and τ_2 were about 0.1 sec, while T was 1 min, so the wing moved with constant velocity U_0 almost throughout its path.

The wing had a symmetrical cross section [5], which on a model for a homogeneous unbounded ideal liquid would mean that the flow pattern was equivalent to that for a point source with strength $q/\pi U_0 D = 0.5$ and a sink having the same total capacity uniformly distributed between points 1 and 2, which are displaced from the source in the U_0 direction by distances $a_1/D = 0.25$ and $a_2/D = 5.4$ (D is the wing thickness, with those parameters corresponding to elongation $\ell_1/D = 6$).

The basic adjustable parameters were δ/b and $Fr = 2\pi(2+\varepsilon)U_0^2/\varepsilon g\delta$, which were varied in the ranges $0.34 \leq \delta/b \leq 5.5$ and $0.5 \leq Fr \leq 100$. The others were chosen such that the wave pattern was as simple as possible in the absence of the barrier. For example, h/δ was taken quite large to minimize the effects on the wave from the hydrodynamic wake behind the wing, while τ_1/T and τ_2/T were small so that the law of (1.2) could be approximated by a stepped function.

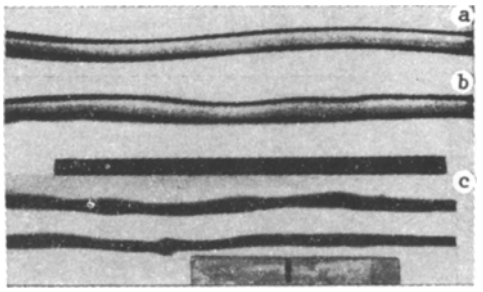

Fig. 3

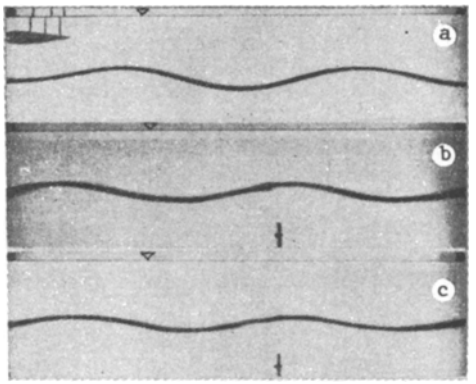

Fig. 4

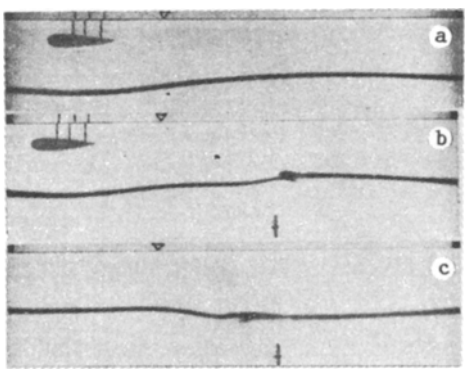

Fig. 5

The wave processes were recorded by cinematography and also by two immobile wave meters 3. The visualization was provided by an ink solution of given density. The meters recorded the conductivity between two vertical electrodes, the output signal e(t) being related to the density $\rho(y, t)$ by

$$e = e_0 + C \int_{y_1}^{y_2} \rho \, dy$$

(e_0 and C are constants, while y_1 and y_2 are the ordinates for the lower and upper ends of the electrodes). Point y_1 was in the lower layer with density ρ_1, and y_2 was in the upper layer having ρ_2, with obedience to the conditions $\delta/(y_2 - y_1) \ll 1$, $\Delta\eta/(y_2 - y_1) \ll 1$ ($\Delta\eta$ is the observed range in the pycnocline fluctuations). Under these conditions, $e \simeq e_0 + C_1\eta$ (η is the deviation in the boundary from the equilibrium position and C_1 = const).

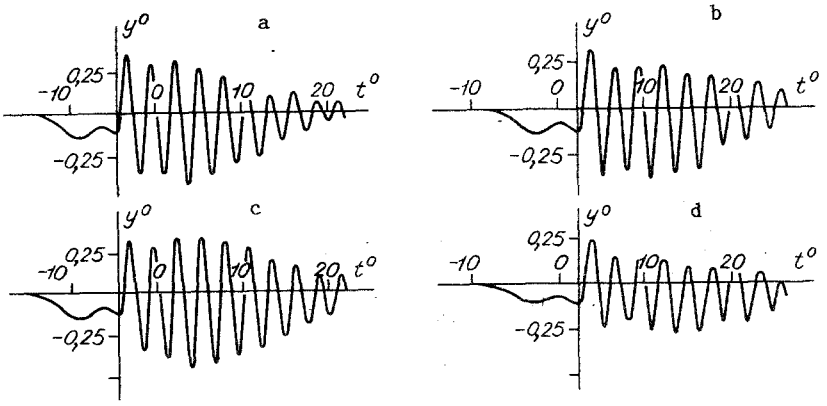

Fig. 6

The waves were damped at the ends by the plate 1 at 4° to the horizontal. Reflection from that plate reduced the wavelength sharply and thus caused rapid viscous attenuation at a rate proportional to k^2 because of the nonlinear processes and the above linear redistribution between modes. The waves reflected from the inclined plate arrived at the nearer wave meter attenuated by more than an order of magnitude.

Fig. 2 shows $\omega_m(k)$ dispersion curves for $m \leq 5$ derived by computation for $\varepsilon = 0.013$, $H_1/\delta = 17.8$, $H_2/\delta = 18$, $\delta = 0.9$ cm (H_1 and H_2 are illustrated by Fig. 1). The $m = 0$ branch corresponds to waves at the free surface, and it almost merges with the ω axis in the (k, ω) region shown in Fig. 2.

These curves enable one to determine the wavelengths, frequencies, and phase and group velocities for the linear stationary harmonic waves excited in the various ways. One needs to plot the characteristic for the corresponding perturbation $\omega_*(k)$ in the (k, ω) plane and examine the points of intersection between it and $\omega_m(k)$. For a steadily moving point source, the perturbation characteristic is provided by the $\omega_* = \pm U_0 k$ rays. In Fig. 2, a indicates such a ray for the typical $U_0 = 6.3$ cm/sec. It intersects the $\omega_1(k)$ branch at (k_1, ω_1) but does not intersect any other $\omega_m(k)$ branches, including the one with $m = 0$, which is due to the surface tension, which means that linear waves in water do not exist for $U_0 < 24$ cm/sec [5]. A ring in stationary motion therefore excites directly only the first internal mode in this example.

The barrier is a source of secondary waves, and it resembles any other immobile obstacle in that the characteristic of this source in the (k, ω) plane is the straight line $\omega_* = \omega_1$ indicated by b in Fig. 2. It intersects all the $\omega_m(k)$ branches, so the barrier interacts with a monoharmonic wave to radiate an infinite set of secondary waves having identical frequency ω_1 but differing lengths $\lambda_m = 2\pi/k_m$. The energy transfer from the basic wave can be to higher or lower modes.

There is a relationship between the k_m for the (1.1) density distribution, which can be put as follows in the asymptotic case $(H_1/\delta, H_2/\delta) \to \infty$:

$$k_{m+1} = k_1 + 2\sqrt{\pi} m \omega_1 / \sqrt{\varepsilon g \delta} \tag{1.3}$$

(g is the acceleration due to gravity). The major parameters are the critical velocities, which are defined by $c^*_m = \lim_{k \to 0} \omega_m/k = \lim_{k \to 0} d\omega_m/dk$. In particular, in the linear theory one can examine only pertrubations whose velocities do not exceed c_m^*. An interesting nonlinear effect for a ring moving with U_0 close to c_m^* is that there are perturbations far ahead of the wing [4].

2. Figure 3 illustrates some effects arising from internal waves interacting with a broad threshold, where part a is for the absence of a threshold with $H_1^0 = 8$, $H_2^0 = 8.1$, $h^0 = 4.8$, $\delta^0 = 1.7$, $\varepsilon = 0.011$, $U_0 = 6.4$ cm/sec and $t_* = 16$ sec (the superscript 0 means that the corresponding quantity is normalized to $D = 2$ cm, while t_* is the time from the start of wing motion). The picture relates to the range in x where the barrier is subsequently placed. Two thin layers are colored, which are symmetrically placed with respect to the boundary and are separated by 0.75δ. The synchronism in the oscillations in those layers confirms that the wing excites only the first internal mode in the absence of the barrier.

Figure 3b is for a barrier with length $\ell^0 = 24$ immersed at $b^0 = 2.9$ and used with $U_0 = 6.6$ cm/sec and $t_* = 34$ sec. The other parameters are as in Fig. 3a, while the time at which the leading edge of the wing passed above the right-hand vertical boundary of the threshold (Fig. 1) was $t_1 = 26$ sec. Here the synchronism between the oscillations in the tagged layers is disrupted and one can clearly see higher modes, where estimates from (1.3) indicate that the barrier excites the mode with m = 2 most extensively.

Figure 3c is for a shorter barrier having $\ell^0 = 12$, $H_1^0 = 7$, $H_2^0 = 11$, $b^0 = 2.1$, $h^0 = 6.5$, $\delta^0 = 3.4$, $\varepsilon = 0.012$, $U_0 = 5.5$ cm/sec, $t_* = 65$ sec ($t_1 = 33$ sec). Here the barrier excites several modes extensively, and the effect is so substantial that local instability occurs in the internal waves.

Figures 4 and 5 show the effects from a barrier with a sharp edge. In Fig. 4, $H_1^0 = 9$, $H_2^0 = 5$, $h^0 = 3.5$, $\delta^0 = 1.4$, $\varepsilon = 0.012$, $U_0 = 5.1$ cm/sec. The colored layer with thickness about 0.5δ lies near the boundary. Picture a is for no barrier with $t_* = 40$ sec, where the first two wave ridges behind the ring have virtually attained the stationary state. In this example, there are no explicit constraints on the scope for describing the waves from the linear theory, since this U_0 is much less than $c^*_1 = 7.5$ cm/sec and the wave slope $a/\lambda \approx 0.05$ is quite small (a is amplitude and λ wavelength). In particular, the wavelength $\lambda_e^0 = 17.2$ in picture a agrees well with that predicted by the linear theory for the first mode, $\lambda_1^0 = 19.1$. Figure 4b is for a barrier with $b^0 = 2$, $t_* = 49$ sec ($t_1 = 6.6$ sec). There is local thickening in the colored layer near the barrier, which over time degenerates into a burst of waves much shorter than the main wave. These secondary waves rapidly degenerate because of the viscosity. They can be traced in not very prominent form in picture c, which applies for this example with $t_* = 56$ sec.

When U_0 lies near c_m^*, nonlinear effects become important and the barrier effect on-creases (Fig. 5), as is evident from experiments under conditions here analogous to those for Fig. 4, apart from $U_0 = 8.0$ cm/sec, which is somewhat more than $c_1^* = 7.5$ cm/sec. Part a is without a barrier at $t_* = 23$ sec. The waves generated by the ring are stable but clearly nonsinusoidal. Ahead of the wing, there are strong perturbations, whose leading edge propagates at a speed in excess of U_0. Parts b and c are with the barrier for $t_* = 23.2$ and 29.2 sec correspondingly. After the wing has passed over, there are liquid flows varying in intensity and direction from one side of the barrier to the other, which is accompanied by local stability loss and a marked change in wave shape. A large part of the energy in the wave motion is dissipated in mixing.

The internal waves are reflected at the barrier without change in length, as in a uniform-density liquid. This is well recorded by the wave meters. Figure 6 shows the signals from them without the barrier and with a barrier with a sharp edge for $H_1^0 = 8$, $H_2^0 = 8.1$, $b^0 = 1$, $h^0 = 4$, $\delta^0 = 0.45$, $\varepsilon = 0.013$, $U_0 = 5.3$ cm/sec, $U_0/c_1^* = 0.59$, $t_* - t_1 = 45$ sec. The abscissa is the dimensionless time $t^0 = \varepsilon g t_1/U_0$, reckoned from the time when the leading edge of the wing passes over the barrier, while the ordinate is the deviation in the boundary from the equilibrium position y^0 normalized to D. The y^0 axis in each recording has been brought into coincidence with the instant when the leading edge of the wing passes over the wave meter.

Parts a and b of Fig. 6 are for no barrier, and c and d for the barrier; a and c are derived from the wave meter placed before the barrier with $x^0 = 12$, while b and d are beyond the barrier for $x^0 = -6$. On account of differences in wave-meter sensitivity, the scale of the recordings along the y^0 axis for $x^0 = 12$ is somewhat larger than that for $x^0 = -6$.

The recordings without the barrier show [6] that the wing-generated perturbations are bursts of waves propagating with speed U_0 and having characteristic wavelength λ_1 and modulated by a longer wave, which is not described by the linear theory even for $U_0 < c^*_1$. The leading edge of the long wave runs continuously ahead of the wing and propagates in this example with speed c^*_1. The leading edge of the perturbations ahead of the wing take the form of a discontinuous wave with undulations or what is called an undulation bore. As time passes, the numbers of ridges and hollows in the undulation bore ahead of the wing increase. In Fig. 6, two depressions are formed ahead of the wing. A series of experiments was performed with $U_0 = 3.5$ cm/sec and $H_2^0 = 4$ together with the above values for the other parameters, when ahead of the wing there was an undulation bore containing four depressions at time $\varepsilon g t_*/U_0 = 260$.

The wave bunch having wavelength λ_1 exists only behind the wing. As time passes, an increasing number of ridges and depressions will attain the stationary state, and new waves arise at the trailing edge. The oscillations in this train are damped because of the combined effects from nonstationarity and viscosity [6].

The waves ahead of the barrier are accentuated by it, and those behind it are attenuated. In the present example, the largest amplitude for the reflected waves constitutes about 25% of that for the incident ones. When the reflected and incident waves are superimposed, the seventh wave recorded by the sensor at $x^0 = 12$ is amplified by a factor 1.7 and the ninth by a factor 2.1. The maximum amplitude beyond the barrier for the transmitted wave at $x^0 = -6$ is less by 28%. The intensity of the perturbations ahead of the wing are reduced by about the same amount. At large times, the waveform and wavelength in the main train behind the wing are altered behind the barrier.

We also performed a series of experiments in which the wing moved between the barrier with the sharp edge and the interface. Here the effects from the hydrodynamic wake behind the wing caused the distortion of the internal-wave pattern by the barrier to be accentuated. The higher-mode excitation in the stratified liquid resulted in more rapid wave-energy dissipation at the obstacle than is the case for a homogeneous medium. In particular, modes may be excited at the obstacle that are unstable in the shear flow generated by the longer waves. The stability loss is accompanied by additional wave energy consumption in the mixing. That process occurs at the barrier for fairly wide ranges in the parameters. Also, even stable higher-mode oscillations are damped rapidly because of the viscosity.

The energy transformation in a stratified medium has a further feature. Not all the energy consumed in the mixing ultimately becomes heat, as part of it goes to increase the potential energy of the system as a whole, as the center of mass is displaced upwards when a stable density stratification becomes uniform.

An interesting feature of this interaction with an obstacle in an inhomogeneous medium is that the obstacle under certain conditions produces an effect very far away along the vertical from the perturbation source. In these experiments, we found the interval-wave disruption at a broad threshold even for $b^0 + h^0 = 15$, and that was far from being the limit.

The effects from the threshold are the more pronounced the larger $Fr\delta/h$ and δ/b; ℓ is also important for a barrier with a broad threshold. Numerical calculations have been made [7] on surface-wave propagation in a homogeneous liquid above a recess at the bottom of a channel with length ℓ, and it was found that there were were minima in the wave transmission coefficient for ℓ/λ multiples of 0.5.

The authors are indebted to I. V. Sturova, whose program was used in the dispersion-curve calculations.

LITERATURE CITED

1. L. H. Larsen, "Internal waves incident upon a knife edge barrier," Deep-Sea Res., 16, No. 5 (1969).
2. R. M. Robinson, "Effect of a vertical barrier on internal waves," Deep-Sea Res., 16, No. 5 (1969).
3. A. A. Korobkin and I. V. Sturova, "Surface and internal wave generation in a variable-depth liquid," in: Hydrophysical Research Methods: Proc. Third All-Union Seminar, Svetlogorsk, May 1989 [in Russian], Inst. Prikl. Fiz. Akad. Nauk SSSR, Gorkii (1990).
4. V. I. Bukreev and N. V. Gavrilov, "An experimental study on the perturbations ahead of a wing moving in a stratified liquid," Zh. Prikl. Mekh. Tekh. Fiz., No. 2 (1990).
5. N. E. Kochin, I. A. Kibel', and N. V. Roze, Theoretical Hydromechanics [in Russian], Vol. 1, Fizmatgiz, Moscow (1963).
6. V. I. Bukreev, A. V. Gusev, and I. V. Sturova, "Nonstationary motion of a circular cylinder in a two-layer liquid," Zh. Prikl. Mekh. Tekh. Fiz., No. 6 (1983).
7. J. J. Lee and R. M. Ayer. "Wave Propagation over a rectangular trench," J. Fluid Mech., 110, (1981).